ARTICLE TYPE www. rsc.org/xxxxxx | XXXXXXXX

# Appendix A - Quantitative Analysis of Optical Losses in Hematite Photoelectrochemical Cell†

**Peter Cendula,[a,‡] Ludmilla Steier,[b‡], S. David Tilley,[b,¶], Matthias Schmid,[a], Matthew T. Mayer,[b], Michael Grätzel,[b], Jürgen O. Schumacher[a]**

***Received Xth XXXXXXXXXX 20XX, Accepted Xth XXXXXXXXX 20XX***
***First published on the web Xth XXXXXXXXXX 200X***
**DOI: 10.1039/b000000x**

The optical losses in a photoelectrochemical (PEC) cell account for substantial part of the solar-to-hydrogen conversion losses, but their quantitative analysis is sparse partially because the optical losses cannot be measured directly in the experiment and their quantification requires accurate knowledge of optical constants of all individual layers. In this work, we present detailed analysis of the optical losses of typical PEC cell based on the combination of spectroscopic measurements and an optical model of both coherent and incoherent layers. We determined wavelength-dependent reflection, transmission and absorption outside of the semiconductor, maximum incident photon-to-current efficiency and charge generation rate. The optical model has been verified for hematite by atomic layer deposition (ALD). Our optical model is a valuable tool for detailed optical loss analysis of a PEC cell and prerequisite for coupled optoelectronic model of a PEC cell.

## 1 Introduction

Photoelectrochemical (PEC) water splitting is a promising pathway for storing solar energy in form of hydrogen.[1–3] The shortcomings of the existing materials lie in the stability, efficiency and cost. To make this approach competitive with other techniques for hydrogen production, PEC water splitting should be achieved without any external voltage bias also known as unassisted water splitting. For this purpose, dual light absorber designs are of great interest,[4–6] since to date no single semiconductor is able to perform unassisted water splitting. In such a design, matching light absorption of the two semiconductors as well as minimal parasitic optical losses outside of the semiconductors are required to achieve the highest internal quantum efficiency. As experimental methods do not provide direct access to the absorptances in the individual layers of a PEC cell, optical modeling (OM) is a powerful tool to make detailed analysis of the wavelength-dependent layer absorptances.

Contrary to other solar cell technologies, modeling and quantification of the optical losses in a typical PEC cell has not yet been addressed extensively[7,8] and only few reports exist in the literature. Han *et al.* optimized quantum efficiencies amorphous silicon double junction solar cells for water splitting with $BiVO_4$ photoanode.[9] A study on the effect of light absorption in aqueous electrolytes on the solar-to-hydrogen (STH) efficiency limitations was presented.[10] Therein, the authors show the dependence of STH efficiency on electrolyte thickness in the PEC cell, however, they do not account for light absorption in other layers of the PEC cell. Another example is the reported increase in light absorption in hematite by light trapping[11] or coating on a nanocone array.[12] Recent literature on modeling of fluid flow, electrochemistry or charge transport is based only on simple Lambert-Beer light absorption, thereby neglecting coherence in thin films[13–16] or disregarding optical processes completely.[17,18]

Hematite ($Fe_2O_3$) is an abundant, cheap, non-toxic PEC semiconductor for water splitting.[19] Although hematite shows slow water oxidation kinetics[20,21] and late photocurrent onset potential,[22,23] hematite water oxidation kinetics continues to be an active research topic.[24] Due to the mismatch of hematite small hole diffusion length ($< 10$ nm) and light penetration depth (several hundred nanometers), nanostructures with high aspect ratio are frequently employed to achieve efficient charge collection.[19,25] One type of the hematite nanostructures is achieved by conformally coating high aspect ratio structures with hematite.[26,27] The atomic layer deposited (ALD) thin film hematite[26] served as a model system for studies with facile one-electron redox couples[?] as compared to aqueous electrolyte (four-electron redox couple)[21] and continues to raise interest with respect to nanostructuring but also forming pn-junctions for enlarged charge collection.[28,29]

To address this lack of optical model-based characterization, we present herein a model of optical light propagation which is capable of quantifying optical losses in all layers of the PEC cell. We describe light propagation in coherent layers (thickness comparable to wavelength of light) with the transfer-matrix method[30] and in incoherent layers (thickness larger than wavelength of light) by ray-tracing geometrical optics.[31,32] Furthermore, we are able to verify our model by ap-

plying it to ALD hematite thin film photoanodes. To obtain a good overlap of the simulated and measured results with our optical model, an accurate and detailed optical characterization of the individual layers - based on their refractive index and extinction coefficient - is essential. Therefore, we first extracted all wavelength-dependent refractive indices and extinction coefficients from spectroscopic ellipsometry and ultraviolet-visible (UV-Vis) spectroscopy measurements and then implemented them in our OM. The proper parametrization of the optical constants is confirmed with the ability of the optical model to reproduce UV-Vis measurements on various test cells. We used validated optical model to calculate spectrally resolved optical losses in the PEC cell and to obtain total integrated optical losses by reflection, transmission and absorption outside of the semiconductor. The charge generation rate from the OM shows limitations of the Lambert-Beer law and can be used in coupled optoelectronic PEC models.

## 2 Theory

In a typical PEC cell configuration as shown in Figure 1 light is interacting with multiple layers (indexed $l$) of different optical properties. Each of the layers needs to be included during optical modeling with accurate complex index of refraction $\tilde{n}_l(\lambda) = n_l(\lambda) + ik_l(\lambda)$, where $n$ is the refractive index, $k$ is the extinction coefficient and $\lambda$ is the wavelength of light. The wavelength dependent absorption coefficient $\alpha(\lambda)$ of layer $l$ is computed from the extinction coefficient by $\alpha_l(\lambda) = \frac{4\pi k_l(\lambda)}{\lambda}$.

Light propagation and absorption in coherent layers are treated with the transfer-matrix method,[30] calculating the propagation of the electric field in the multilayer stack by matrix operations derived from Fresnel equations of all interfaces in the cell. Optical propagation in incoherent layers is described by following geometric light rays and their reflections and transmissions (including attenuation in absorbing media) in the multilayer cell recursively until their intensity drops below a certain threshold.[32] The energy conservation is fulfilled during optical modeling and it holds

$$R_{tot}(\lambda) + \sum_l A_l(\lambda) + T_{tot}(\lambda) = 1, \qquad (1)$$

where $R_{tot}$ is the total reflectance, $A_l$ denotes absorptance of layer $l$ and $T_{tot}$ is the total transmittance.[30,33]

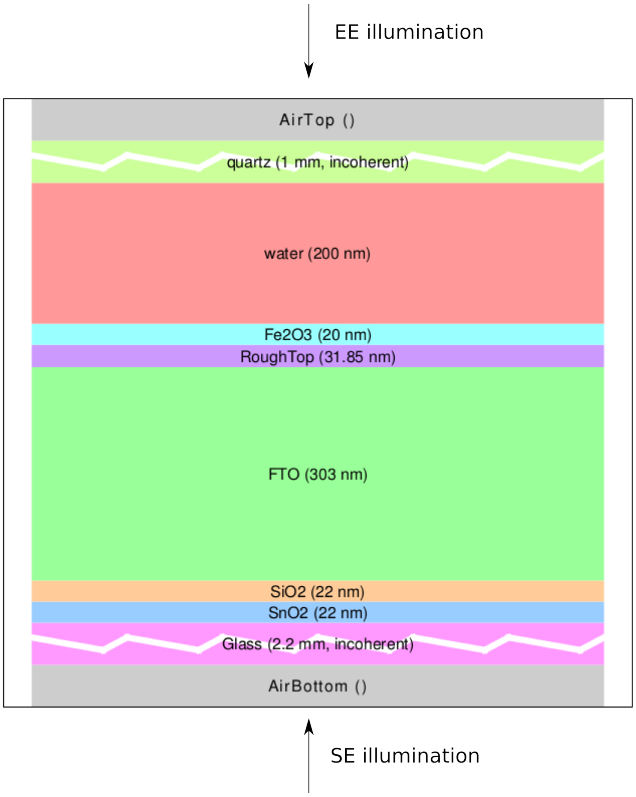


**Fig. 1** Sketch of the PEC cell layer sequence used for UV-Vis measurements and simulations. Thicknesses of the layers are scaled for the purpose of presentation.

† Electronic Supplementary Information (ESI) available: [details of any supplementary information available should be included here]. See DOI: 10.1039/b000000x/

[a] *Institute of Computational Physics, Zurich University of Applied Sciences (ZHAW), Wildbachstrasse 21, 8401 Winterthur, Switzerland. Tel: +41-58-934-7796; E-mail: cend@zhaw.ch*

[b] *Laboratory of Photonics and Interfaces, Ecole Polytechnique Fédérale de Lausanne, EPFL-SB-ISIC-LPI, Station 6, 1015 Lausanne, Switzerland.*

‡ These authors contributed equally to this work.

¶ Present address: Department of Chemistry, University of Zurich, Winterthurerstrasse 190, 8057, Zurich, Switzerland.

The rough/porous layer is described with Bruggemann effective medium approximation

$$P\frac{n_a^2-n_e^2}{n_a^2+2n_e^2}+(1-P)\frac{n_b^2-n_e^2}{n_b^2+2n_e^2}=0, \quad (2)$$

where medium $a$ is enclosed in medium $b$ with fraction $P$ (porosity) and resulting effective medium has an effective refractive index $n_e$.

The presented optical losses can be quantified also in terms of photocurrent, if we assume ideal conversion of every photon to separated electron-hole pair. The photocurrent loss by reflection, transmission and absorption is calculated by integrating the product of $R_{tot}$, $T_{tot}$ and $A_l$ with the incident spectral photon flux $\phi(\lambda)$ of AM15G illumination [34]

$$\{j_R, j_{A_l}, j_T\} = q\int_\lambda \{R_{tot}(\lambda), A_l(\lambda), T_{tot}(\lambda)\}\phi(\lambda)\mathrm{d}\lambda, \quad (3)$$

where $q = 1.602\cdot 10^{-19}$ C is the electronic charge.

Proper understanding of the optical absorption in the PEC cell from our optical model allows us to calculate the number of absorbed photons in any position in the semiconductor per unit volume and time. We further assume that every absorbed photon generates a single electron-hole pair. Hence, the charge generation rate in the semiconductor calculated from OM is given by

$$G_{OM}(x) = \int_\lambda \frac{\alpha(\lambda)I(\lambda,x)}{E(\lambda)}\mathrm{d}\lambda, \quad (4)$$

where $I(\lambda,x)$ is the energy flux at position $x$ calculated from the optical model, $E(\lambda)=\frac{hc}{\lambda}$ is the photon energy, $h = 6.626\cdot 10^{-34}$ kg·m$^2$/s is the Planck constant and $c = 299792458$ m/s is the speed of light in vacuum. The $x$ coordinate has its origin at the hematite/water interface and is positive towards hematite. The charge generation rate is frequently assumed to obey the simple Lambert-Beer law and neglects reflection and parasitic absorption in layers above the semiconductor (water, quartz). Full AM15G spectral photon flux is assumed to impinge on the semiconductor

$$G_{LB}(x) = \int_\lambda \alpha(\lambda)\phi(\lambda)e^{-\alpha(\lambda)x}\mathrm{d}\lambda. \quad (5)$$

Clearly, Lambert-Beer law is insufficient to describe multilayer cells where the amount of light entering the buried layer is much lower than the light impinging on the whole cell.

We assume optical properties of the actual electrolyte are equal to those of water. Both illuminations from the electrolyte-electrode (EE) or substrate-electrode (SE) are considered.

# 3 Experimental

## 3.1 Atomic-layer deposition

$Fe_2O_3$ was deposited by atomic layer deposition (ALD) in a home-built ALD reactor at 230 °C (0.025 nm/cycle) using dimethylaminomethylferrocene (Alfa Aesar, 98+% pure, bubbler heated to 90 °C) and ozone (x% $O_3$ in $O_2$ (99.9999% pure) produced by an ozone generator (xx)) as described elsewhere. [35]

For the different optical measurements, three different substrates have been used: F:SnO2 (TCO22-15, Solaronix SA, Switzerland), Quartz (Ted Pella, USA) or n-Si wafers coated with a thin ALD layer of $TiO_2$ (1.5 nm) to provide a common substrate interface between the three substrates used. At the same time the thin underlayer induces n-doping into the thin hematite film and mitigates the known problem of photoinactive thin films in hematite called the dead layer effect. [36] The $TiO_2$ layer was deposited in the home-built reactor at 170 °C with a growth rate per cycle of 0.06 nm/cycle using (TDMAT) (bubbler heated to 75 °C) and water as precursors. The TCO22-15 substrates were cleaned by successive ultra-sonication for 15 min with acetone, soap, water and 2-propanol as previously reported. [37]

## 3.2 Spectroscopic ellipsometry

For the optical characterization of the TCO22-15 (Solaronix SA, Switzerland) ellipsometry was measured on two TCO22-15 clean samples. Sample 1 was covered with Zn powder and immersed into a 2 M HCl solution to etch the F:$SnO_2$ from the float glass. The glass was rinsed with water and 2-propanol and dried in air. Sample 2 remained unchanged. Ellipsometry data was measured with a GES 5e (Sopra, France) and analyzed with WinEli software applying Cauchy-Lorentz and standard dielectric function dispersion laws. The internal structure of the TCO22-15 glass was analyzed by means of ellipsometry with the help of cross-sectional transmission electron micrographs (Fig. S2†). For the extraction of the optical constants of each layer, the thicknesses were fixed to the ones observed by TEM and listed in the following: glass (2.2 mm), $SnO_2$ (18 nm), $SiO_2$ (18 nm), F:$SnO_2$ (303 nm), Void/$SnO_2$ mixture with 94.08% void (32 nm) to account for surface roughness and porosity. For the extraction of the optical constants of hematite and the $TiO_2$ underlayer, ellipsometry measurements were carried out on n-Si wafers as well as on quartz.

## 3.3 UV-Vis measurements

Spectrally resolved total reflectance $R_{tot}$ , total transmittance $T_{tot}$ and diffuse reflectance were measured with a UV-3600 spectrometer (Shimadzu Scientific Instruments, USA). Before

the measurement the sample was rinsed with water and dried in air to remove any dust particles, and placed in a sandwich type configuration between two quartz slides in water before inserting in the beam path of the integrating sphere of the spectrometer. All measurements were carried out in EE and SE orientation in a wavelength range of 300 nm to 800 nm.

## 4 Results

We will use following notation to simplify description of our different test multilayers: TCO22-15 (T), quartz (Q), water (W), hematite (H). The layer sequence on Fig. 1 with EE light illumination direction will be denoted by QWHTiT, the light in our notation always impinges from the left. Hence, in our notation THWQ denotes SE illumination of QWHTiT. We also note that the internal layer structure of the TCO22-15 (T) consists of rough layer $SnO_2$/void(94%) (Ro), F:$SnO_2$ (F), $SiO_2$ (Si), $SnO_2$ (Sn) and float glass (G).

First, the optical constants of the individual layers of the photoelectrode (Q, H, F, Si, Sn, G) were determined by combination of literature values and parameter extraction from spectroscopic ellipsometry and UV-Vis spectroscopy (Supporting Information text and Figures S1-S9 †). The extracted optical constants of ALD hematite from spectroscopic ellipsometry with HQ layers are shown on Figure 2. The extinction coefficient for our ALD hematite is larger than reported by Martinson *et al.* [26] pointing to the film deposition differences even between two different ALD fabrication setups. The refractive index our ALD hematite was compared with literature profile from ... as Ref. 26 did not contain refractive index data.

### 4.1 Verification of the optical model

We assembled multilayers QWHTiQ and QWHTiT in order to confirm predictive abilities of our OM and we obtained good overlap of the reflectance and transmittance measurements and simulations for EE illumination, Figure 3 (comparison for SE illumination is available in Supporting Information †). The transmittance of QWHTiQ is ≈0.4 for 300 nm $< \lambda <$ 400 nm wavelengths and increases then to ≈0.9 at $\lambda$ =700 nm as a consequence of light absorption in hematite in this wavelength range. The reflectance of QWHTiQ is ≈0.2 for 300 nm $< \lambda <$ 600 nm and then decreases to ≈0.1 at $\lambda$ =800 nm due to the large mismatch of refractive index of water/hematite interface ($\frac{n_W}{n_H} \approx \frac{1.35}{2.9}$). The transmittance of QWHTiT and QWHTiQ show similar profile and the QWHTiT reflectance for 300 nm $< \lambda <$ 400 nm reproduces correct valley and peak positions and magnitude of the measured specular $R_{spec}$ reflectance. The total reflectance consists of the specular and diffusive reflectance $R_{tot} = R_{spec} + R_{diff}$.

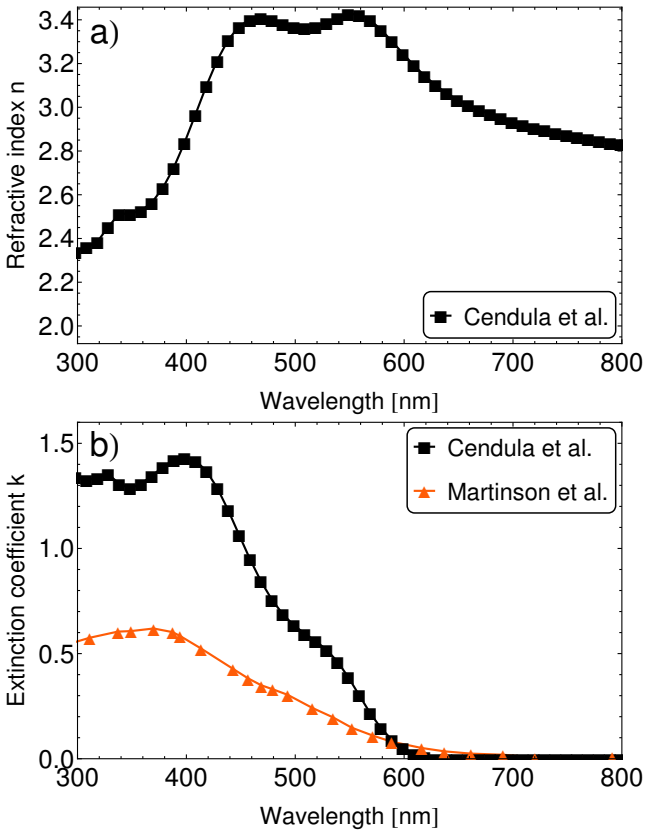


**Fig. 2** Optical constant of hematite extracted from ellipsometry of two layers HQ, a) refractive index and b) extinction coefficient.

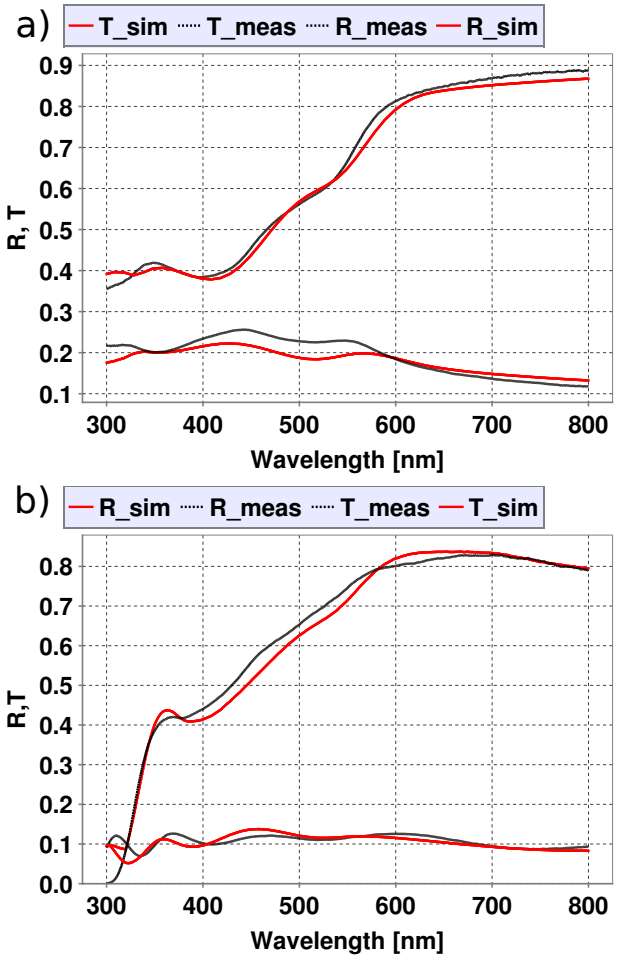


**Fig. 3** Comparison of measured (black) and fitted (red) reflectance and transmittance of 12 nm ALD hematite, EE illumination for a) QWHTiQ and b) QWHTiT.

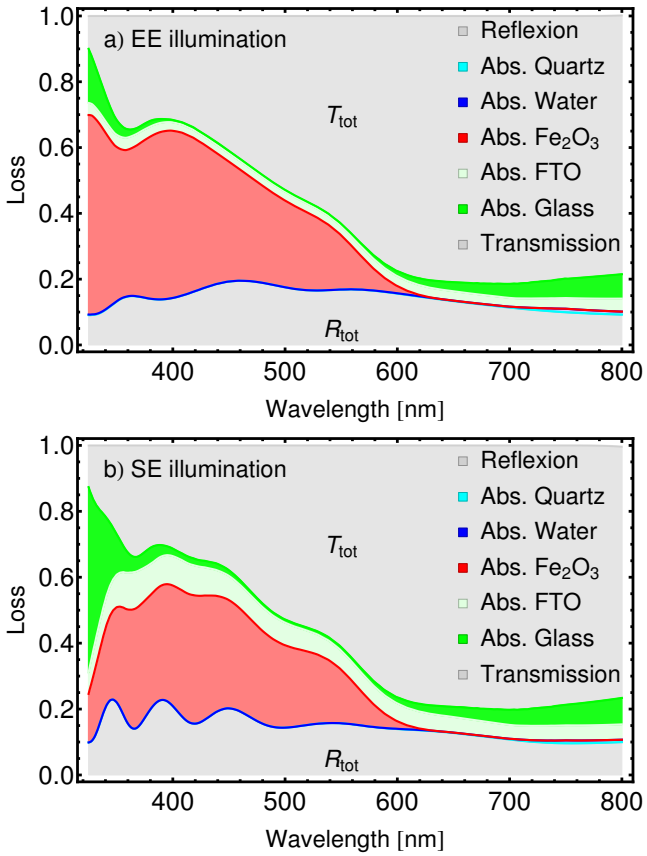


**Fig. 4** Detailed optical loss analysis of a PEC cell with a) EE and b) SE illumination. The calculated total reflectance, the absorptance in each layer and the total transmittance are stacked and colored in the graphs.

### 4.2 Optical loss analysis

Having validated our optical model with measurements, we investigated optical propagation in the ?cappuccino? PEC cell as used for photocurrent measurements at LPI EPFL.[22,36,38] The thickness of ALD hematite is 12 nm and thickness (width) of electrolyte in this cell is 0.4 cm. Valuable insight into the optical losses in the individual layers is presented on Figure 4. The calculated reflectance $R_{tot}$, absorptances in the individual layers $A_l$ and transmittance $T_{tot}$ for EE and SE illumination are shown in stacked diagram and satisfy the energy conservation eq. 1. For every wavelength $\lambda$, different ratio of illumination energy is reflected, absorbed in individual layers or transmitted through the PEC cell and strongly depends on the illumination direction.

For EE illumination, Figure 4a, the absorptance in hematite is ≈0.4-0.5 for 300 nm $< \lambda <$ 400 nm, afterwards decreasing to zero near $\lambda$ =600 nm (corresponding to wavelength of its

bandgap energy). Nearly constant absorption loss of ≈0.1 can be seen for $SnO_2$:F over whole wavelength range and glass absorption is largest for $\lambda < 350$ nm (up to ≈0.2) and for $\lambda > 600$ nm (which is uncritical given the cease of hematite absorption for $\lambda > 600$ nm). The absorption in water and quartz is negligible in the presented data.

For SE illumination, Figure 4b, the absorptance in hematite for $\lambda$ <400 nm is smaller compared to EE illumination due to much stronger absorption in float glass which stands in the SE light path before hematite. Absorption in $SnO_2$:F for SE illumination is slightly larger than for EE illumination. Reflectance for both EE and SE illumination makes ≈0.1-0.2 but the interference fringes of $SnO_2$:F are more pronounced for the SE illumination. Decrease in reflectance losses from ≈0.2 to ≈0.04 could be achieved by using anti-reflective coatings with established techniques.[30]

Table 1 shows the integrated losses in terms of photocurrents eq. 3 corresponding to different physical processes in the PEC cell. The sum of these respective channels gives the maximum possible photocurrent for hematite ≈12.5 mA/cm$^2$.

| Optical loss | EE [mA/cm$^2$] | EE [%] | SE [mA/cm$^2$] | SE [%] |
|---|---|---|---|---|
| Reflection | 2.1 | 17 | 2.0 | 16 |
| Abs. Quartz | 0 | 0 | 0 | 0 |
| Abs. Water | 0 | 0 | 0 | 0 |
| Abs. Hematite | 3.5 | 28 | 3.0 | 24 |
| Abs. $SnO_2$:F | 0.3 | 3 | 0.9 | 7 |
| Abs. Glass | 0.1 | 1 | 0.3 | 3 |
| Transmission | 6.4 | 51 | 6.2 | 50 |

**Table 1** Optical loss channels for 12 nm ALD hematite in terms of photocurrent.

### 4.3 Absorptance in hematite

The absorptance in the hematite layer $A_{Fe2O3}$ is in close relation to the incident photon-to-current efficiency (IPCE) which gives ratio of number of electrons in external circuit divided by the number of incident photons on the device. If we assume that every absorbed photon in hematite layer contributes electron in the external circuit (absorbed photon-to-current efficiency $APCE = 1$) then the absorptance in the hematite is equal to the maximum theoretically achievable IPCE according to

$$IPCE_{max} = A_{Fe2O3}, \quad (6)$$

which follows from eq. 7 $IPCE_{max}$ from our optical simulations is larger than our measured $IPCE$ data at 1.43 V vs. RHE due to the inefficient collection of photogenerated charges (most of them recombine before contributing to photocurrent), Figure 5. The values of $IPCE_{max}$ are only upper limit of achievable IPCE in ideally collecting hematite photoelectrode

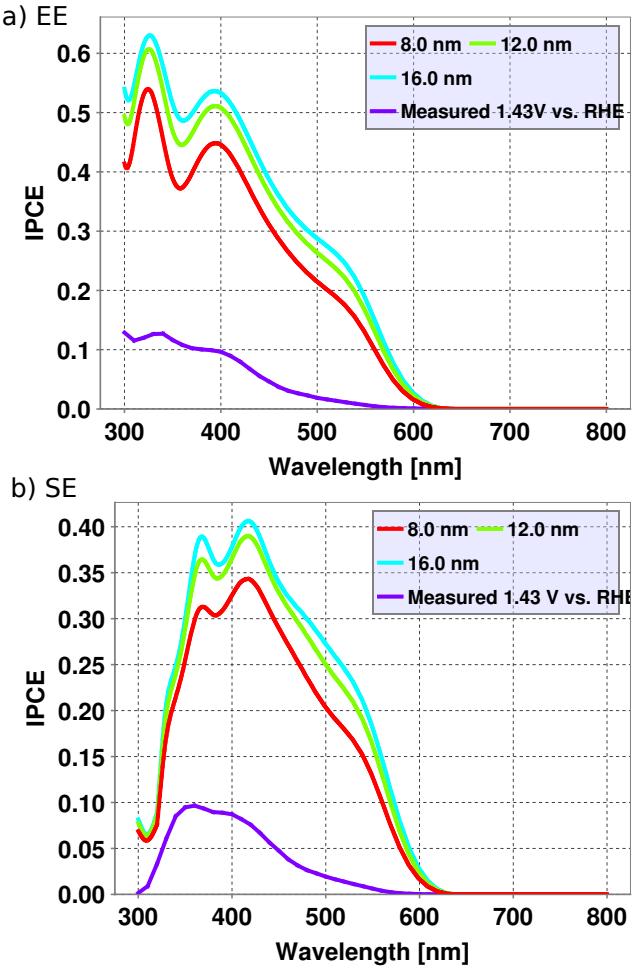


**Fig. 5** Calculated $IPCE_{max}$ of hematite films for thicknesses 8 nm, 12 nm, 16 nm and our measured IPCE data at 1.43 V vs. RHE. a) EE and b) SE illumination.

which is readily not the case of our photoelectrode. For increasing thickness of hematite 8, 12, 16 nm, the $IPCE_{max}$ increases only slightly, but for much larger hematite thickness (¿ 50 nm) there are substantial gains in the hematite absorptance in the visible absorption (Supporting Information Fig. S13 †). However, keeping in mind the hole diffusion length of 2-4 nm reported for hematite,[39] thicknesses larger than 4 nm suffer from inefficient charge transport, thereby, decreasing the photoelectrochemical performance.

The calculated absorptance in hematite $A_H$ can be used to calculate APCE from IPCE data, but without the usual simplifying assumption $APCE = IPCE\frac{I_0}{I_0-I}$ with $I_0$ the initial input light intensity and $I$ is the output light intensity of UV-Vis measurement.[5,25,40] For monochromatic illumination, the APCE is calculated from absorbed power $P_{abs}$ in analogy to IPCE (which uses incident light power $P_{in}$)[7]

$$APCE(\lambda) = \frac{hc}{q}\frac{j_{ph}(\lambda)}{P_{abs}(\lambda)\lambda} = IPCE(\lambda)\frac{P_{in}(\lambda)}{P_{abs}(\lambda)} = \frac{IPCE(\lambda)}{A_H}, \quad (7)$$

where $j_{ph}$ is the measured photocurrent. Calculation of APCE will be investigated in the future together with optoelectronic model of IPCE measurement.

### 4.4 Charge generation rate

The optical model is now used to calculate $G_{OM}(x)$ charge generation profile and compare it with the Lambert-Beer charge generation profile $G_{LB}(x)$ for EE illumination, Figure 6. Since thickness of the ALD hematite used in this study (12 nm) is small compared to the wavelength of light, the hematite layer is described as coherent. The charge generation rate from the OM is smaller than from the LB because the absorption of light is less effective in coherent than in incoherent layers. The LB formula is valid only for incoherent layers,[41,42] which we recovered by our OM calculations. The charge generation rate $G_{OM}(x)$ will be used as direct input for electrical model of the photoelectrode and thus enable coupled optoelectronic modeling of the photoelectrode.

## 5 Conclusions

We presented an optical model of light absorption in all layers of a typical PEC cell setup. Light propagation in the incoherent layers was described by geometrical ray tracing and in the coherent layers by transfer-matrix method. The optical model was validated with UV-Vis and ellipsometry measurements. We calculated wavelength-dependent losses in individual layers of the PEC cell which is not possible with direct measurements. The optical losses were given also as total integrated lost photocurrent for both illumination directions. The

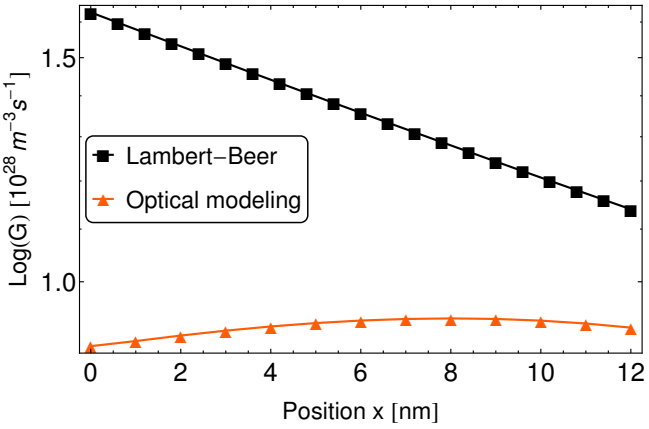


**Fig. 6** Comparison of charge generation rate in the semiconductor (logarithmic scale) calculated from Lambert-Beer $G_{LB}(x)$ (linear) and from optical modeling $G_{OM}(x)$.

poor measured IPCE performance of ALD hematite compared to absorptance in ALD hematite indicates the large room for improvement. The accurate optoelectronic modeling of thin PEC photoelectrode cannot include simple Lambert-Beer law assumption for charge generation rate but rather needs charge generation rate to be determined from optical modeling. The wavelength-dependent quantification of optical losses in PEC cells will allow detailed optimization of optical absorption and electrical collection in dual-absorber PEC cells and systems.

## 6 Acknowledgements

We thank G. Rothenberger and N. Téetreault (both LPI EPFL) for experimental help and fruitful discussions and Fluxim AG for technical support. The financial support by the Swiss Federal Office of Energy (PECHouse2 project, contract number SI/500090-02) is gratefully acknowleged. Please add your funding sources

## References

1 M. G. Walter, E. L. Warren, J. R. McKone, S. W. Boettcher, Q. Mi, E. A. Santori and N. S. Lewis, *Chem. Rev.*, 2010, **110**, 6446–6473.
2 J. Luo, J.-H. Im, M. T. Mayer, M. Schreier, M. K. Nazeeruddin, N.-G. Park, S. D. Tilley, H. J. Fan and M. Grätzel, *Science*, 2014, **345**, 1593–1596.
3 M. Grätzel, *Nature*, 2001, **414**, 338–344.
4 M. S. Prévot and K. Sivula, *The Journal of Physical Chemistry C*, 2013.
5 R. V. D. Krol and M. Grätzel, *Photoelectrochemical Hydrogen Production*, Springer, 2011.
6 J. Brillet, M. Cornuz, F. L. Formal, J.-H. Yum, M. Grätzel and K. Sivula, *Journal of Materials Research*, 2010, **25**, 17–24.
7 G. Dennler, K. Forberich, M. C. Scharber, C. J. Brabec, I. Tomiš, K. Hingerl and T. Fromherz, *Journal of Applied Physics*, 2007, **102**, 054516.

8 K. Ding, T. Kirchartz, B. E. Pieters, C. Ulbrich, A. M. Ermes, S. Schicho, A. Lambertz, R. Carius and U. Rau, *Solar Energy Materials and Solar Cells*, 2011, **95**, 3318–3327.

9 L. Han, F. F. Abdi, P. P. Rodriguez, B. Dam, R. v. d. Krol, M. Zeman and A. H. M. Smets, *Physical Chemistry Chemical Physics*, 2014, **16**, 4220–4229.

10 H. Döscher, J. F. Geisz, T. G. Deutsch and J. A. Turner, *Energy & Environmental Science*, 2014.

11 H. Dotan, O. Kfir, E. Sharlin, O. Blank, M. Gross, I. Dumchin, G. Ankonina and A. Rothschild, *Nature Materials*, 2012.

12 K. X. Wang, Z. Yu, V. Liu, M. L. Brongersma, T. F. Jaramillo and S. Fan, *ACS Photonics*, 2014.

13 L. Andrade, T. Lopes, H. A. Ribeiro and A. Mendes, *International Journal of Hydrogen Energy*, 2011, **36**, 175–188.

14 A. Berger and J. Newman, *Journal of The Electrochemical Society*, 2014, **161**, E3328–E3340.

15 P. Cendula, S. D. Tilley, S. Gimenez, M. Schmid, J. Bisquert, M. Graetzel and J. O. Schumacher, *Journal of Physical Chemistry C*, 2014, **DOI:10.1021/jp509719d**, year.

16 H. S. Park, H.-W. Ha, R. S. Ruoff and A. J. Bard, *Journal of Electroanalytical Chemistry*, 2014, **716**, 8–15.

17 S. Haussener, C. Xiang, J. M. Spurgeon, S. Ardo, N. S. Lewis and A. Z. Weber, *Energy & Environmental Science*, 2012, **5**, 9922.

18 C. Carver, Z. Ulissi, C. Ong, S. Dennison, G. Kelsall and K. Hellgardt, *International Journal of Hydrogen Energy*, 2012, **37**, 2911–2923.

19 K. Sivula, F. Le Formal and M. Grätzel, *ChemSusChem*, 2011, **4**, 432–449.

20 M. Barroso, A. J. Cowan, S. R. Pendlebury, M. Gra?tzel, D. R. Klug and J. R. Durrant, *J. Am. Chem. Soc.*, 2011, **133**, 14868–14871.

21 B. Klahr, S. Gimenez, F. Fabregat-Santiago, T. Hamann and J. Bisquert, *J. Am. Chem. Soc.*, 2012, **134**, 4294–4302.

22 S. D. Tilley, M. Cornuz, K. Sivula and M. Grätzel, *Angewandte Chemie*, 2010, **122**, 6549–6552.

23 C. Du, X. Yang, M. T. Mayer, H. Hoyt, J. Xie, G. McMahon, G. Bischoping and D. Wang, *Angewandte Chemie International Edition*, 2013, **52**, 12692–12695.

24 F. Le Formal, 2015.

25 I. Cesar, K. Sivula, A. Kay, R. Zboril and M. Grätzel, *J. Phys. Chem. C*, 2008, **113**, 772–782.

26 A. B. F. Martinson, M. J. DeVries, J. A. Libera, S. T. Christensen, J. T. Hupp, M. J. Pellin and J. W. Elam, *The Journal of Physical Chemistry C*, 2011, **115**, 4333–4339.

27 J. Brillet, M. Gra?tzel and K. Sivula, *Nano Letters*, 2010, **10**, 4155–4160.

28 M. T. Mayer, Y. Lin, G. Yuan and D. Wang, *Accounts of Chemical Research*, 2013.

29 M. T. Mayer, C. Du and D. Wang, *Journal of the American Chemical Society*, 2012, **134**, 12406–12409.

30 H. A. Macleod, *Thin-Film Optical Filters, Third Edition*, CRC Press, 2001.

31 J. Krc and M. Topic, *Optical Modeling and Simulation of Thin-Film Photovoltaic Devices*, CRC Press, 2013.

32 *SETFOS 4.0, www.fluxim.com*, 2014.

33 S. Wenger, M. Schmid, G. Rothenberger, A. Gentsch, M. Gra?tzel and J. O. Schumacher, *J. Phys. Chem. C*, 2011, **115**, 10218–10229.

34 NREL, *Solar Spectral Irradiance: Air Mass 1.5 (accessed March 17, 2012), http://rredc.nrel.gov/solar/spectra/am1.5/*.

35 L. Steier, 2015.

36 L. Steier, I. Herraiz-Cardona, S. Gimenez, F. Fabregat-Santiago, J. Bisquert, S. D. Tilley and M. Grätzel, *Advanced Functional Materials*, 2014, n/a–n/a.

37 F. Le Formal, M. Grätzel and K. Sivula, *Advanced Functional Materials*, 2010, **20**, 1099–1107.

38 J. Brillet, J.-H. Yum, M. Cornuz, T. Hisatomi, R. Solarska, J. Augustynski, M. Graetzel and K. Sivula, *Nature Photonics*, 2012, **6**, 824.

39 J. H. Kennedy, *Journal of The Electrochemical Society*, 1978, **125**, 709.

40 Z. Chen, T. G. Deutsch, H. N. Dinh, K. Domen, K. Emery, A. J. Forman, N. Gaillard, R. Garland, C. Heske, T. F. Jaramillo, A. Kleiman-Shwarsctein, E. Miller, K. Takanabe and J. Turner, *Photoelectrochemical Water Splitting*, Springer New York, 2013, pp. 87–97.

41 M. Born and E. Wolf, *Principles of Optics: Electromagnetic Theory of Propagation, Interference and Diffraction of Light*, CUP Archive, 2000.

42 R. Santbergen, A. H. Smets and M. Zeman, *Optics Express*, 2013, **21**, A262–A267.

# Supporting information for: Quantitative Analysis of Optical Losses in Hematite Photoelectrochemical Cell

Peter Cendula,*,† Ludmilla Steier,‡ S. David Tilley,‡ Matthias Schmid,† Matthew T. Mayer,‡ Michael Grätzel,‡ and Jürgen O. Schumacher†

*Institute of Computational Physics, Zurich University of Applied Sciences (ZHAW), Wildbachstrasse 21, 8401 Winterthur, Switzerland, and Laboratory of Photonics and Interfaces, Ecole Polytechnique Fédérale de Lausanne, EPFL-SB-ISIC-LPI, Station 6, 1015 Lausanne, Switzerland*

E-mail: cend@zhaw.ch

## Determination of optical constants of individual layers of the photoelectrode stack

### Quartz (Q)

The UV-Vis measurement of plain quartz sample agrees with optical simulations, Figure S1.

*To whom correspondence should be addressed
†Zurich University of Applied Sciences
‡Ecole Polytechnique Fédérale de Lausanne

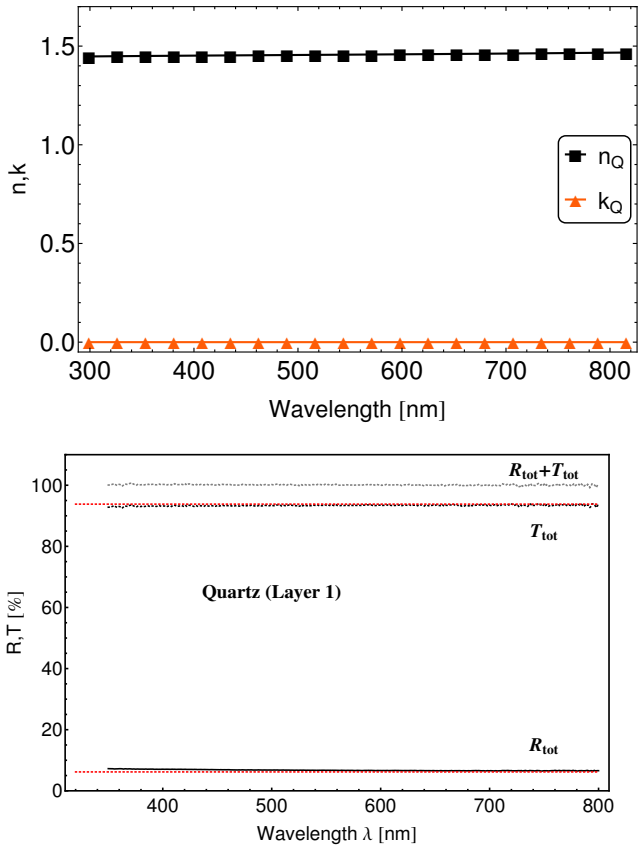


Figure S1: (top) Optical constants used for quartz. (bottom) Comparison of measured and simulated T and R spectra of quartz.

## Water (W)

Optical constants of water in 300-800 nm wavelength range are nearly constant with $n_W \approx 1.35$ and $k_W \approx 0$, Figure S2.

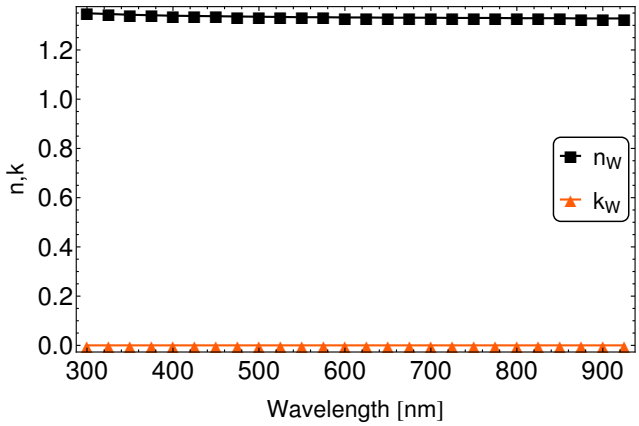


Figure S2: Optical constants of water taken from Ref. S1.

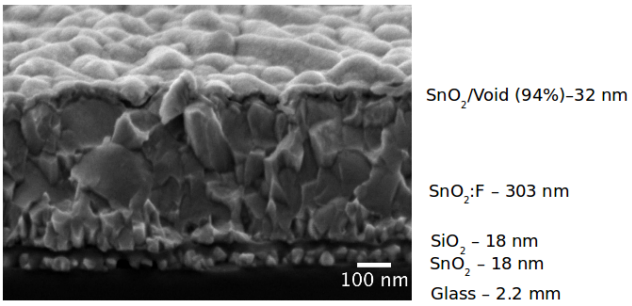


Figure S3: Cross-section TEM image of glass substrate TEC15 showing its internal structure with approximate thicknesses determined by eye.

## TEC15 substrate (T)

The glass substrate used for PEC cells (TCO22-15 from Solaronix) consists the rough layer $SnO_2$/void(94%) (Ro), $SnO_2$:F (F), $SiO_2$ (Si), $SnO_2$ (Sn) and float glass (G) as described in the main text with short notation RoFSiSnG. The internal structure of the TEC15 was revealed by scanning electron microscopy, Figure S3.

### Float Glass (G)

The optical constant of the float glass were determined as follows. First, the top F layer was etched away to measure reflectance $R_{exp}$ and transmittance $T_{exp}$ of the actual float glass with planar surfaces[S2] in the integrating sphere. The complex refractive index of the float glass $\tilde{n}(\lambda) = n(\lambda) + ik(\lambda)$ is connected with the total reflectance $R_{tot}$ and transmittance $T_{tot}$ with relations[S2]

$$R = \frac{(n-1)^2 + k^2}{(n-1)^2 + k^2}, \quad (1)$$

$$\alpha = \frac{4\pi k}{\lambda}, \quad (2)$$

$$R_{tot} = \frac{R(1 + (1-2R)e^{-2\alpha d})}{1 - R^2 e^{-2\alpha d}}, \quad (3)$$

$$T_{tot} = \frac{(1-R)^2 e^{-\alpha d}}{1 - R^2 e^{-2\alpha d}}. \quad (4)$$

We obtained $n(\lambda), k(\lambda)$ separately for every wavelength by solving system of two equations $R_{exp} = R_{tot}$ and $T_{exp} = T_{tot}$, Fig. S4.

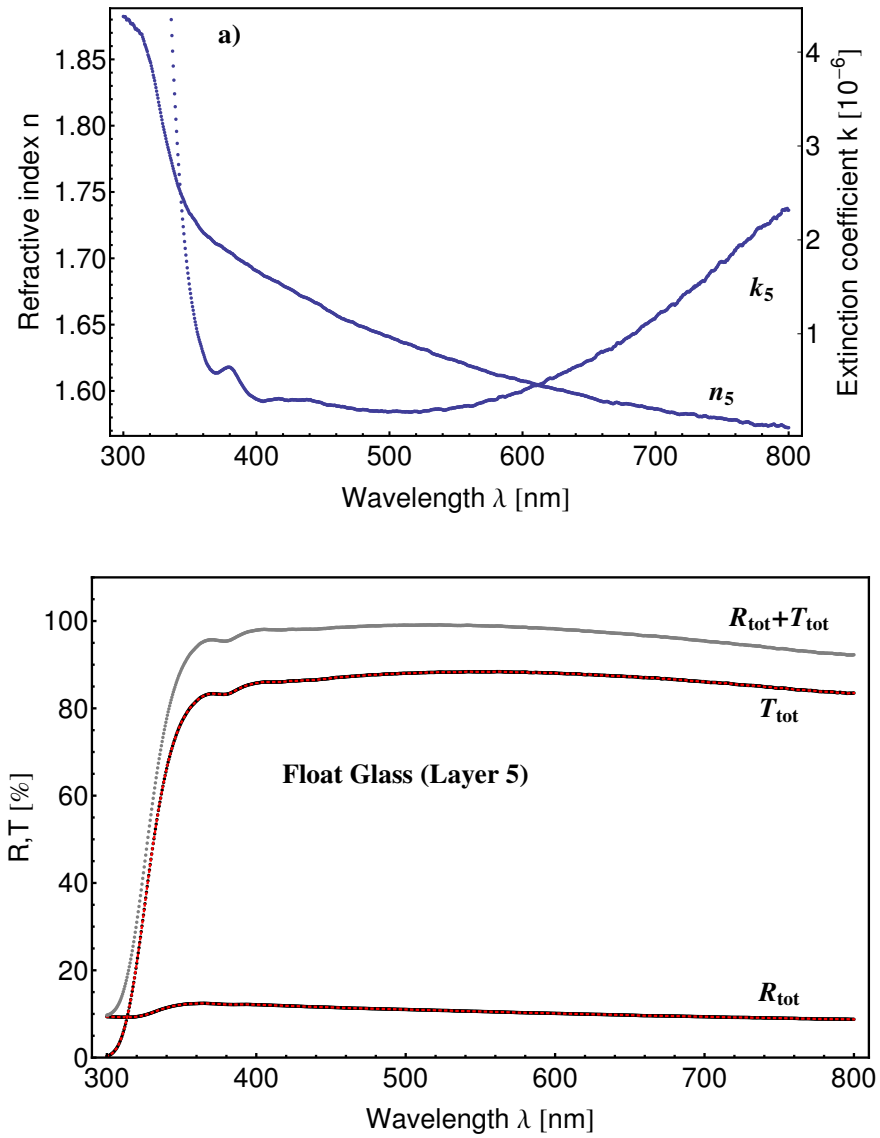


Figure S4: a) Extracted optical constants of the float glass. b) Comparison of measured (black) and simulated (red) T and R spectra of the float glass.

### $SnO_2$ (Sn)

Optical constants of $SnO_2$ are shown on Figure S5.

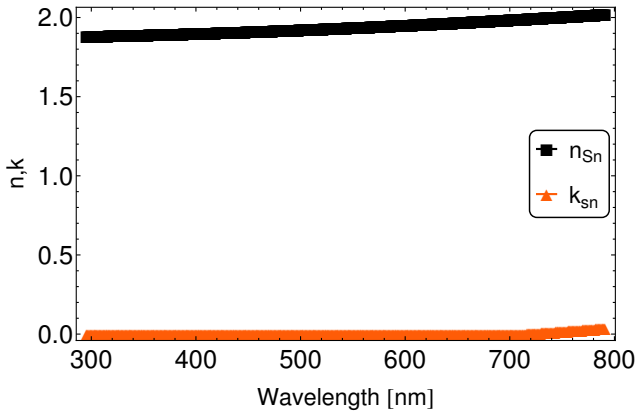


Figure S5: Optical constants of $SnO_2$ extracted from spectroscopic ellipsometry.

### $TiO_2$ (Ti)

Optical constants of $TiO_4$ are shown on Figure S6.

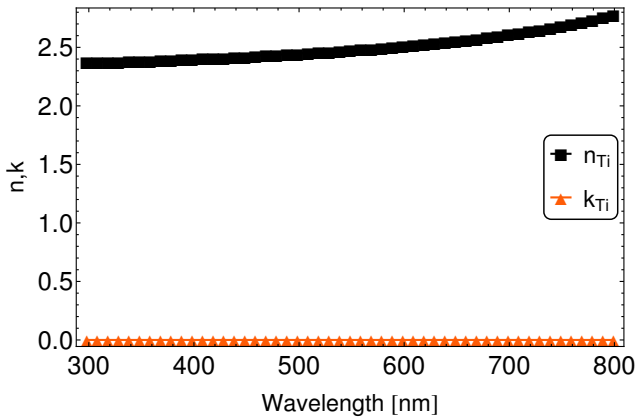


Figure S6: Optical constants of $TiO_2$ extracted from spectroscopic ellipsometry.

### $SnO_2$:F (F)

Having determined the $n, k$ of the glass contained in TEC15 Glass in the previous section, we extracted the optical constants of $SnO_2$/void (94percent), $SiO_2$ and $SnO_2$ from spectroscopic ellipsometry, Figure S7.

We fitted the optical constants of F so as to obtain overlap of transmittance measurements and simulations, Figure S8.

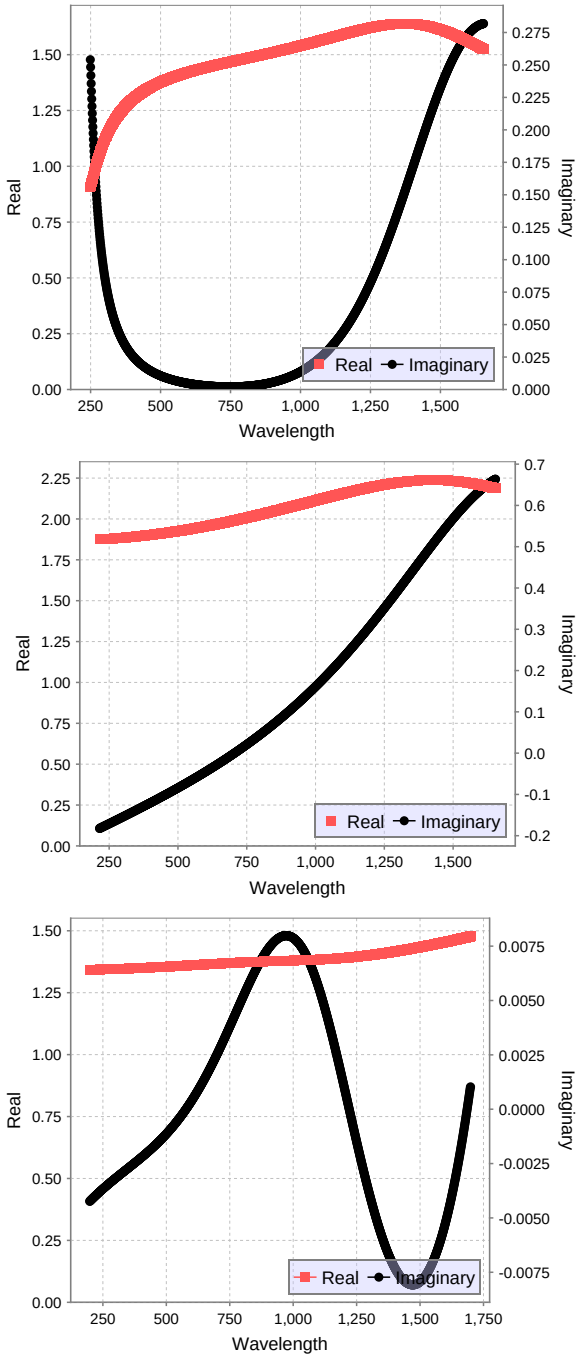


Figure S7: Optical constants determined from ellipsometry : (1st) F:$SnO_2$+Void effective medium with 94% roughness, (2nd) $SnO_2$, (3rd) $SiO_2$.

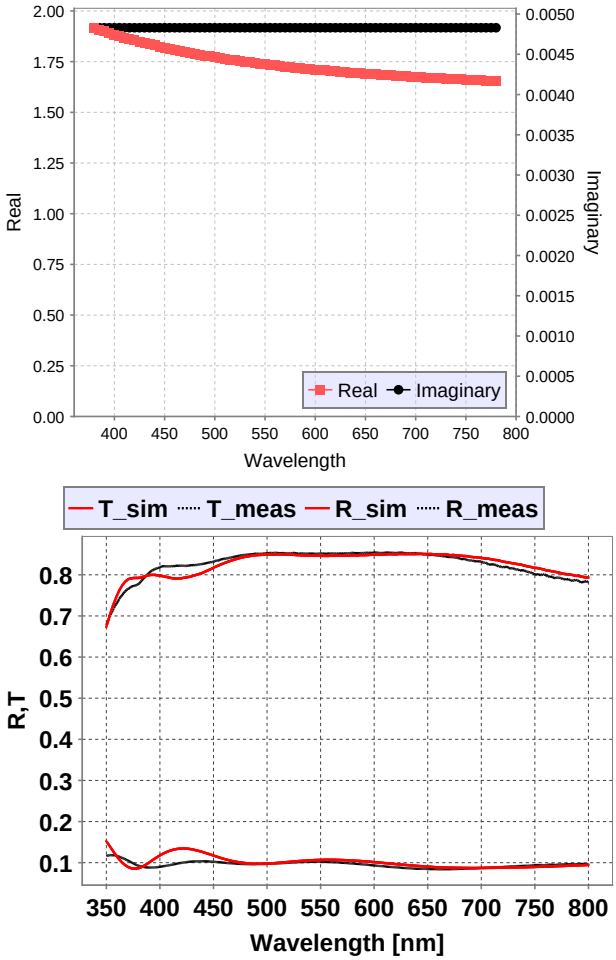


Figure S8: (top) Extinction coefficient of F found by numerical optimization for fixed refractive index profile. (bottom) Comparison of measured (black) and fitted (red) reflectance and transmittance of TEC15.

## Hematite stacks

We first tested the optical constants of hematite deposited by ALD on a $TiO_2$ coated quartz substrate (HTiQ). The good agreement of the UV-vis measurements and simulations confirms accuracy of our optical constant for $Fe_2O_3$, Figure S9.

As a following step, we deposited hematite on TEC15 and compared Uv-Vis measurements and simulations, Figure S9. We could not obtain good overlap with the thickness of hematite estimated from deposition on quartz (12 nm, 500 cycles), as there was 10-15% less transmittance in the simulated data. The reason might lie in the conformal nature of ALD deposition of hematite on the effectively larger rough surface of TEC15 (cf. Fig. S3 ) as compared to flat surface of quartz. Since the amount of deposited material is the same but the effective area is larger, we assumed 'effective thickness' of hematite on rough TEC15 surface to be 8 nm instead of 12 nm (500 cycles) and we obtained more reasonable overlap of the measured and simulated UV-Vis data, Figure S9. Also, F is difficult to coat most probably because of it's fluorine content and therefore the growth rate in the first layers is not the same as on Si or quartz.

The absorptance in individual layers of the QWHTiT cell are shown on Figure S10.

Reasons why we didn't included IPCE measurements of Ludmilla's hematite: - doped TiO2 underlayer makes the disagreement between magnitude of photocurrent-voltage (EE¡SE) and IPCE for (EE¿SE). Since one should show both IV and IPCE together in a paper, this is not suitable. Ability of the photoelectrode to convert light of various wavelengths to electrical current is quantified in the incident photon-to-current efficiency (IPCE), which is synonym to external quantum efficiency (EQE). IPCE couples effect of three processes in PEC: 1) the fraction of electron–hole pairs generated per incident photon flux ($\eta_{e^-/h^+}$), 2) charge transport to the solid–liquid interface ($\eta_{transport}$), and 3) the efficiency of interfacial charge transfer ($\eta_{interface}$)[S3]

$$IPCE(\lambda) = \eta_{e^-/h^+}\eta_{transport}\eta_{interface}. \quad (5)$$

The IPCE is typically obtained from chronoamperometry by measuring the photocur-

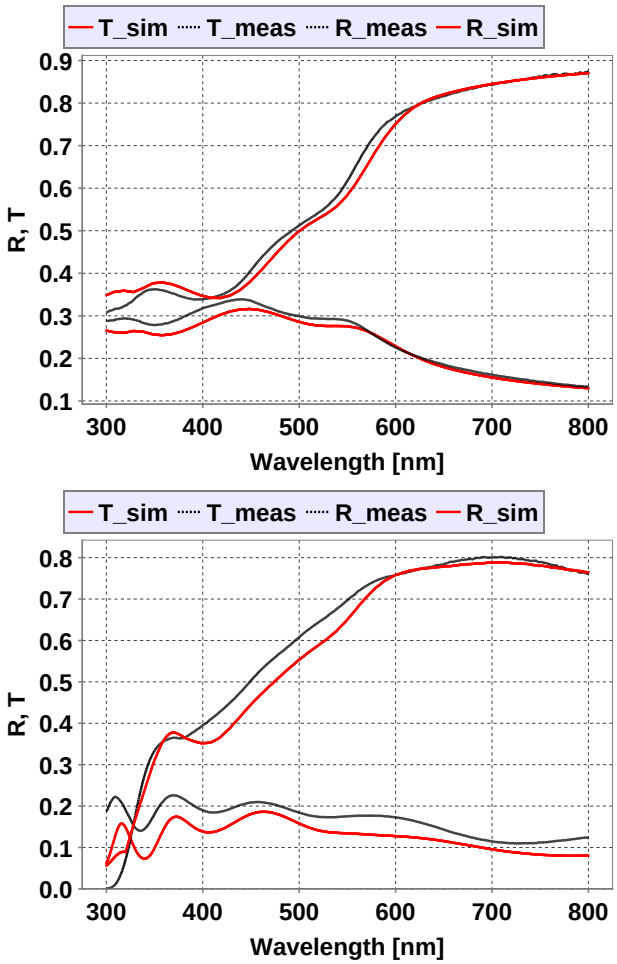


Figure S9: (top) Comparison of measured (black) and fitted (red) reflectance and transmittance of 12 nm ALD hematite on quartz (HTiQ). (bottom) Comparison of measured (black) and fitted (red) reflectance and transmittance of 8 nm ALD hematite on TEC15 (HTiT).

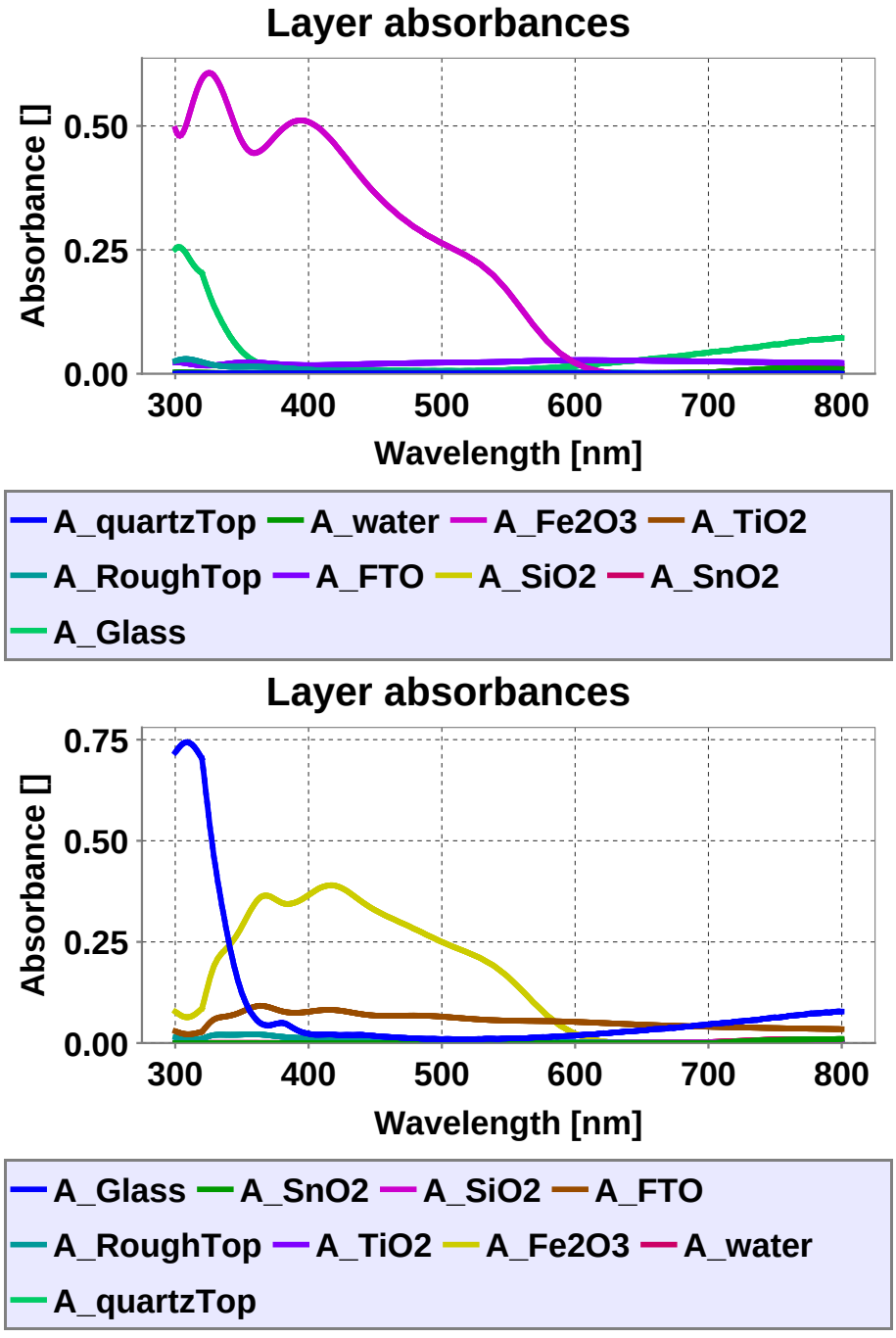


Figure S10: The absorptance in individual layers of the QWHTiT cell for (top) EE and (bottom) SE illumination.

rent $j_{ph}$ extracted from the photoelectrode while illuminating with light power $P_{in}$

$$IPCE(\lambda) = \frac{hc}{q}\frac{j_{ph}(\lambda)}{P_{in}(\lambda)\lambda}, \tag{6}$$

where $h = 6.626 \cdot 10^{-34}$ J·s denotes Planck's constant, $c = 299792458$ m/s is speed of light in vacuum and $q = 1.602 \cdot 10^{-19}$ C is the electronic charge.

By isolating the optical reflection and transmission of the photoelectrode stack $\eta_{e^-/h^+}$ from the IPCE, one obtains absorbed photon-to-current efficiency (APCE), which is synonym to internal quantum efficiency (IQE). APCE relates the collected photocurrent per number of absorbed photons and gives the inherent performance of the photoelectrode material[S3]

$$APCE(\lambda) = \frac{IPCE(\lambda)}{\eta_{e^-/h^+}} = \eta_{transport}\eta_{interface}. \tag{7}$$

The traditional assumption when calculating APCE in the literature on hematite[S4–S9] is that number of electron-hole pairs generated equals number of photons absorbed and leads to expression[S10,S11]

$$A = -\log\left(\frac{I}{I_0}\right), \tag{8}$$

$$\eta_{e^-/h^+} = \frac{I_0 - I}{I_0} = 1 - 10^{-A}, \tag{9}$$

$$APCE(\lambda) = \frac{IPCE(\lambda)}{1 - 10^{-A}}, \tag{10}$$

where $A$ is the absorbance of the electrode, $I_0$ is the initial input light intensity and $I$ is the output light intensity of UV-Vis measurement. However, the internal layer structure of the photoelectrode is disregarded during this assumption and parasitic absorption (in the other layers of photoelectrode then hematite) is neglected. Hence, the estimated absorbance $A$ of the semiconductor is overestimated.

Therefore more detailed model of absorptance in the individual layers is necessary in order to obtain accurate APCE values. Calculated APCE will shed light into largest loss channels in the photoelectrode.

To relax the assumptions for APCE calculation above, we present here optical model

which disentangles the parasitic absorption within the cell.

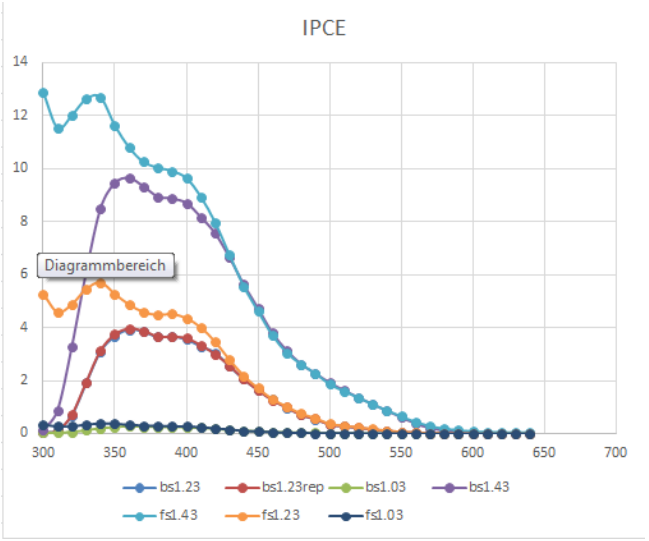


Figure S11: IPCE for SE is smaller than for EE below 350 nm because of absorption of TEC15 (same as for BiVO4, krol p.100). Matt+Ludmilla don't know why the IPCE of EE(fs) is higher than SE(bs) when the current is actually higher for SE than for EE (opposite situation). 500cycles Fe2O3=8(12) nm hematite. First compute APCE after formula from SI,[S7] second compute APCE from optical model.

Measurement of IPCE of ALD hematite.[S8]

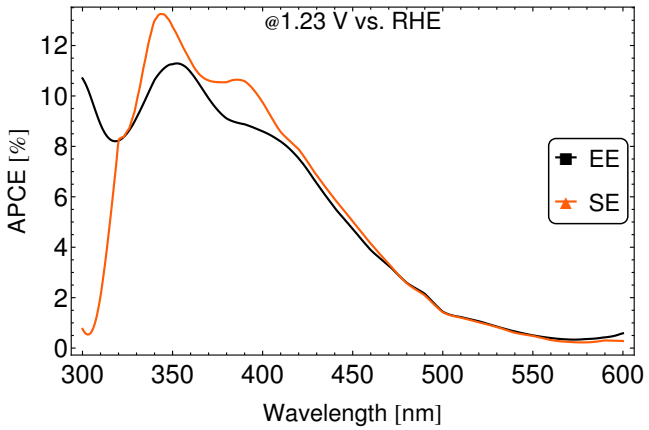


Figure S12: APCE spectra for EE or SE calculated after eq. **??** have similar profile.

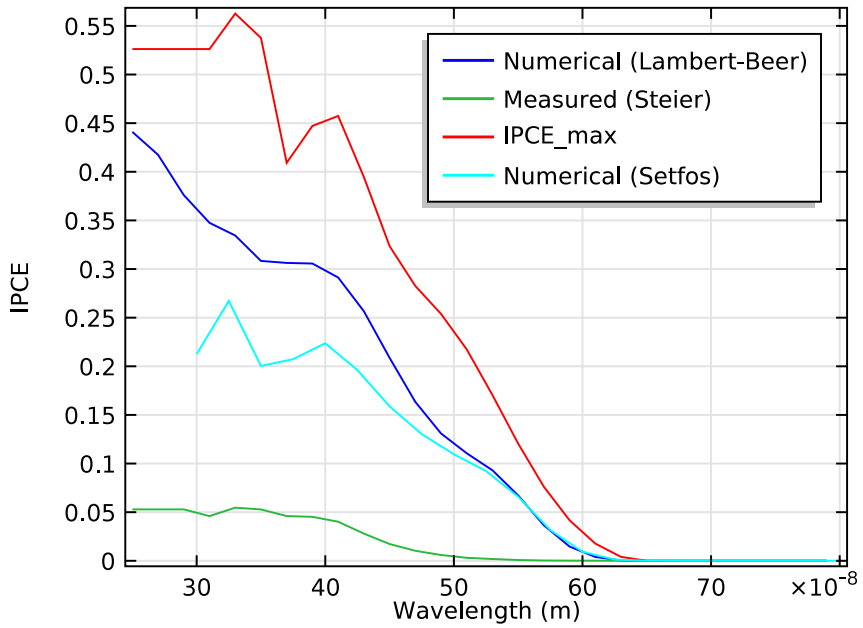


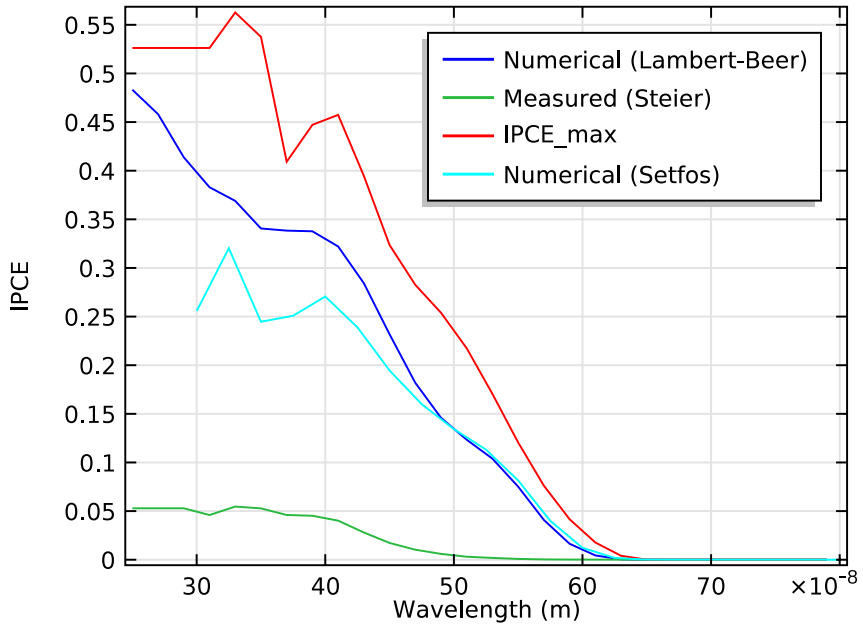


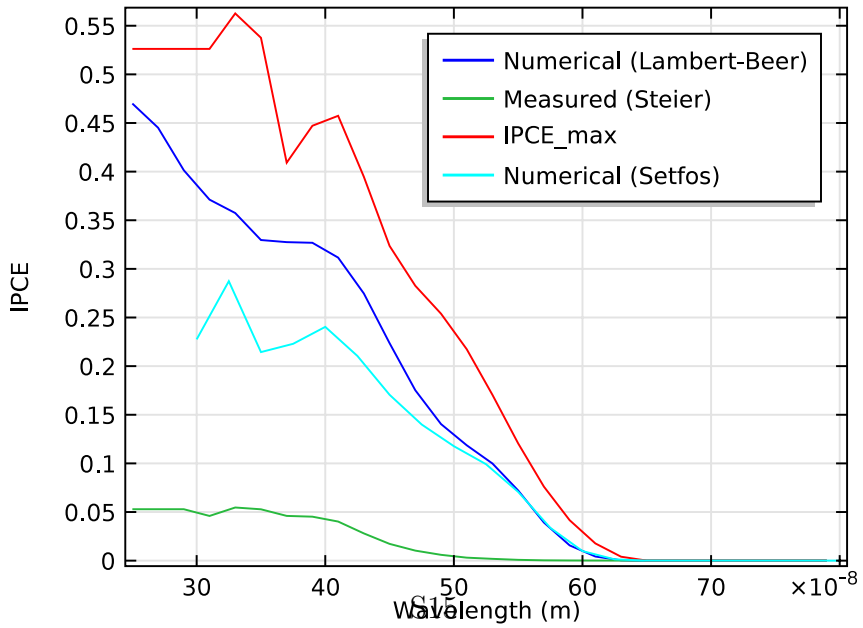




Figure S13: IPCE spectra for EE and 0.8 V vs. RHE (top) 1.0 V vs. RHE (middle) and

# Optical loss analysis

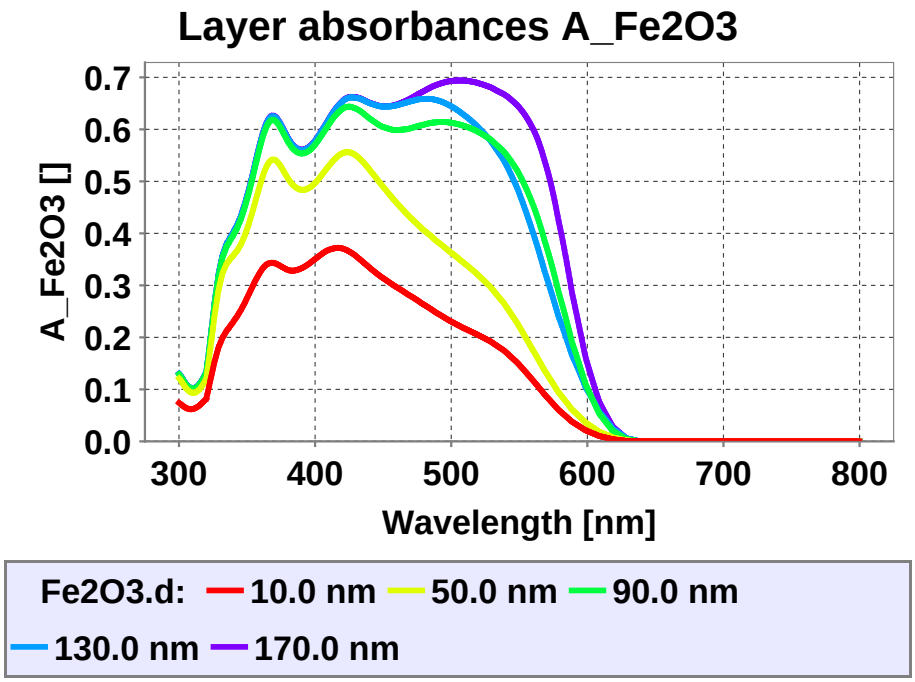


Figure S14: Calculated $IPCE_{max}$ of hematite films for large thicknesses 10 nm to 170 nm and SE illumination.

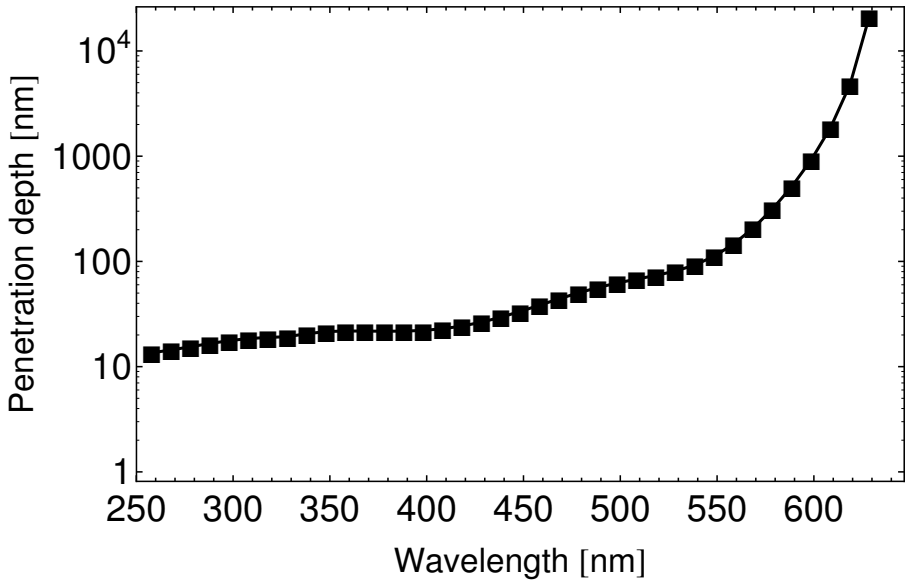


Figure S15: Penetration depth $\alpha^{-1}$ in hematite calculated from the extinction coefficient in Figure 2 of the main text. For wavelengths around 300-400 nm, the penetration depth is between ≈ 10-20 nm, which explains good absorptance of 10 nm hematite film around 300-400 nm wavelengths, Fig. S15. For wavelengths around above 500 nm, the penetration depth rises fast to ≈100 nm, hence we find better absorptance of hematite above 400 nm wavelength for films thicker than 100 nm, Fig. S15.

## References

(S1) Hale, G. M.; Querry, M. R. *Applied Optics* **1973**, *12*, 555.

(S2) Wenger, S.; Schmid, M.; Rothenberger, G.; Gentsch, A.; Gra?tzel, M.; Schumacher, J. O. *J. Phys. Chem. C* **2011**, *115*, 10218–10229.

(S3) Chen, Z.; Deutsch, T. G.; Dinh, H. N.; Domen, K.; Emery, K.; Forman, A. J.; Gaillard, N.; Garland, R.; Heske, C.; Jaramillo, T. F.; Kleiman-Shwarsctein, A.; Miller, E.; Takanabe, K.; Turner, J. *Photoelectrochemical Water Splitting*; SpringerBriefs in Energy; Springer New York, 2013; pp 7–16.

(S4) Cesar, I.; Sivula, K.; Kay, A.; Zboril, R.; Grätzel, M. *J. Phys. Chem. C* **2008**, *113*, 772–782.

(S5) Sivula, K.; Formal, F. L.; Grätzel, M. *Chemistry of Materials* **2009**, *21*, 2862–2867.

(S6) Le Formal, F.; Grätzel, M.; Sivula, K. *Advanced Functional Materials* **2010**, *20*, 1099–1107.

(S7) Hisatomi, T.; Dotan, H.; Stefik, M.; Sivula, K.; Rothschild, A.; Grätzel, M.; Mathews, N. *Advanced Materials* **2012**, *24*, 2699–2702.

(S8) Lin, Y.; Zhou, S.; Sheehan, S. W.; Wang, D. *Journal of the American Chemical Society* **2011**, *133*, 2398–2401.

(S9) Huang, Z.; Lin, Y.; Xiang, X.; Rodríguez-Córdoba, W.; McDonald, K. J.; Hagen, K. S.; Choi, K.-S.; Brunschwig, B. S.; Musaev, D. G.; Hill, C. L.; Wang, D.; Lian, T. *Energy & Environmental Science* **2012**,

(S10) Varghese, O. K.; Grimes, C. A. *Solar Energy Materials and Solar Cells* **2008**, *92*, 374–384.

(S11) Nazeeruddin, M. K.; Kay, A.; Rodicio, I.; Humphry-Baker, R.; Mueller, E.; Liska, P.; Vlachopoulos, N.; Graetzel, M. *Journal of the American Chemical Society* **1993**, *115*, 6382–6390.